

# An analytical model for gold nanoparticle radiosensitisation

Pedro Teles<sup>a,b,\*</sup>

<sup>a</sup>*Departamento de Física e Astronomia da Faculdade de Ciências da Universidade do Porto, Porto, Portugal,*

<sup>b</sup>*Centro de Investigação do Instituto Português de Oncologia do Porto, Porto, Portugal,*

---

## Abstract

In this paper, we derive a variance-driven Local-Effect-Model ( $\sigma$ -LEM) to predict radiosensitization due to gold nanoparticles (AuNP). Assuming that the number of Au photo-ionisations scales strictly with particle volume  $V_{\text{NP}} \propto R^3$  and that the cascade energy deposition is log-normally distributed, the enhanced dose in each target voxel can be written as  $D_{\text{enh}} = D_0 \exp(\sigma Z)$  with  $Z \sim \mathcal{N}(0, 1)$  and width  $\sigma = \sqrt{2 \ln(1 + Kc)}$ .

By assuming a linear-quadratic (LQ) dose response, a relation between survival and dose can be derived for each voxel. Although there is no closed form for the log-normal distribution, averaging over the entire domain using first and second order moments leads to three possible closed forms, a variance-only one, a mixed-term one, where simultaneous hits from enhancement and baseline can occur, and a second-order model, accurate to  $\mathcal{O}(\sigma^3)$ . These three variants adapt well to low-concentration, mid-concentration, and high-concentration regimes.

The model was tested for Bovine aortic endothelial cells (BAEC) results, irradiated with a 100 kVp x-ray beam, taken from a Local Effect Model (LEM) and experimental values. The model shows good agreement with the

---

\*Corresponding author: ppteles@fc.up.pt

experimental data, with deviations within acceptable limits, but presents significant changes to the results obtained with the LEM. In particular, results seem to indicate that dose enhancement is mostly  $\alpha$ -driven. These findings are further developed in the manuscript.

The theoretical framework presented here collapses radiobiological outcomes to two experimentally controllable variables — beam quality, in the term  $K_c$ , and intracellular concentration  $c$ —while retaining mechanistic fidelity. Additional tests should be made to further confirm the validity of the model.

---

## 1. Introduction

Gold nanoparticles (AuNPs) (and other high-Z elements) have been the subject of extensive research for cancer treatment applications [1–4]. When irradiated, due to a heightened photoelectric cross-section coupled with high Auger electron yields, AuNPs enhance the local dose in their surrounding, as produced Auger cascades deposit orders-of-magnitude more energy within tens of nanometres than the original photon beam alone [5–7].

The most effective model to describe AuNP radiosensitization is the Local Effect Model (LEM). LEM was originally developed for heavy-ions, with McMahon *et al.* first modifying it to score nanoscale radial dose profiles of gold nanoparticles (AuNPs), predicting surviving fractions that agreed with clonogenic data for 1.9 nm AuNPs under 105–220 kVp photons [8]. Their analysis showed that the mean number of Au photo-ionisations scales with NP volume ( $V_{\text{NP}} \propto R^3$ ) but also that for equal mass many small NPs seem to have the same biological effect than a few large ones, showing that, besides the AuNP sizes, concentration would play a significant role as well [8].

Lechtman *et al.* combined full-track Monte Carlo (MC) energy deposition around 50 nm AuNPs with a voxelised linear–quadratic (LQ) survival calculation and reproduced prostate-cell SER within 1 % [9].

Similar MC+LQ studies now exist for proton-beam AuNPs [10] and for kilovoltage gadolinium NPs (GdNPs) [11]. These models are very accurate, requiring the calculation of voxel doses using Monte Carlo simulations around the nanoparticle.

In this work, we develop a completely theoretical  $\sigma$ -LEM, derived exclusively from physical first principles, establishing a relationship between beam quality and stochastic local dose enhancement, showing that, at first-order, DER varies exclusively with concentration. By assuming a log-normal distribution for the dose enhancement, we average over the entire domain to obtain closed-form macroscopic equations for DERs and survival curves under different concentration regimes, showing that the first-order moment captures the lower concentrations well, the first-order moment and a mixed term are best suited for intermediate concentrations, and the second-order moment aligns well with higher concentrations.

The developed model was tested with previously published experimental and LEM results [5, 7] yielding good accuracy, although predicting an  $\alpha$ -driven enhancement, different from the prediction of the LEM.

Finally, the  $\sigma$ -LEM model has been developed for x-ray activation, but can potentially be adapted to other beams (protons, heavy-ions).

## 2. Methodology

The  $\sigma$ -LEM model was derived from physical first principles. Spectrum-weighting, fitting, table and figure generation were all performed with the use of python scripts. Experimental BAEC survival data were digitised with WebPlotDigitizer [12]. A single energy-independent constant,  $\varepsilon_{\text{cas}} N_{\text{Auger}} \approx 1 \times 10^{-5} \text{ Gy}$ , was obtained by minimising the Root Mean Square Error between model and synchrotron DERs.

Three analytic survival curves (variance-only, mixed, second-order) were derived by successive expansions in  $\sigma$  and Gaussian averaging, then cast into LQ form by weighted least squares.

### 3. Results

#### 3.1. Baseline ionisations per Gray and primary photo-absorptions in one AuNP

For a broad X-ray field under charged-particle equilibrium (CPE) the homogeneous dose deposited in tissue is

$$D = \left\langle \left( \frac{\mu_{\text{en}}}{\rho} \right)_t E \right\rangle \Phi, \quad (1)$$

where  $E$  is photon energy,  $\Phi$  the incident fluence (photons  $\text{cm}^{-2}$ ), and  $\langle (\mu_{\text{en}}/\rho)_t E \rangle$  is evaluated over the spectrum. Setting  $D = 1 \text{ Gy}$  defines the reference fluence

$$\Phi_{1 \text{ Gy}} = \frac{D_0}{\langle (\mu_{\text{en}}/\rho)_t E \rangle}. \quad (2)$$

In a AuNP, the number of ionizations that occur in it, when traversed by an X-ray beam, is proportional to the number of photons that interact with the AuNP:

$$N_{\text{ion}} = \frac{A_{\text{AuNP}}}{A_{\text{source}}} \cdot (1 - e^{-\langle \mu_{\text{phot}}^{\text{Au}} \rangle \cdot \bar{x}}), \quad (3)$$

where  $A_{\text{AuNP}}$  is the area of the AuNP,  $A_{\text{source}}$  is the area of the source used,  $\langle \mu_{\text{phot}}^{\text{Au}} \rangle$  is the mean photoelectric cross section of gold for the x-ray spectrum, and  $\bar{x}$  is the mean chord length of the AuNP. Considering that  $\bar{x}$  is extremely small, the previous equation is well approximated by the first term of the Taylor expansion, leading to [13]:

$$N_{\text{ion}} = \frac{A_{\text{AuNP}}}{A_{\text{source}}} \cdot \langle \mu_{\text{phot}}^{\text{Au}} \rangle \cdot \bar{x} + \mathcal{O}(\bar{x}^2), \quad (4)$$

Where the terms  $\mathcal{O}(\bar{x}^2)$  are so small they can be neglected.

Considering that the mean chord length is  $\bar{x} = V_{\text{NP}}/A_{\text{NP}}$ , then the number of ionizations per photon is given by:

$$N_{ion} = \frac{A_{AuNP}}{A_{source}} < \mu_{phot}^{Au} > \bar{x} = < \mu_{phot}^{Au} > \frac{V_{AuNP}}{A_{source}}, \quad (5)$$

meaning that the number of ionisations  $N_{ion}$  is proportional to the volume of the AuNP, regardless of its shape, and also that  $N_{ion} \propto R^3$ .

If we multiply equation 5 by equation 2, and by the total number of AuNPs  $N_{AuNP}$ , we obtain the number of ionizations per Gy:

$$N_{ion}^{Gy} = D_0 \cdot \frac{< \mu_{phot}^{Au} >}{\langle (\mu_{en}/\rho)_t E \rangle} \cdot N_{AuNP} \cdot V_{AuNP}. \quad (6)$$

$$= \mathcal{F}(E, t) \cdot N_{AuNP} \cdot V_{AuNP}, \quad (7)$$

where  $\mathcal{F}(E, t)$  represents the number of ionizations per Gy per AuNP per volume of the AuNP and has units of  $\text{cm}^{-3}$ , easily convertible to  $\text{nm}^{-3}$ .

The number of ionisations per Gy is proportional to the volume of the nanoparticle. This has clear implications, like the shape of the NP being irrelevant as long as the volume is the same. Also, because  $V_{NP} \propto R^3$ , the mean cascade dose scales strictly with  $R^3$ . At the same time, this equation tells us that the number of ionisations is proportional to the number of AuNPs.

### 3.2. Log-normal distribution of dose deposition

Experimental studies across many fields have repeatedly shown that the dose deposition by a photoelectron is log-normally distributed [14–18]

In fact, if we assume that the enhanced dose deposited in a scoring voxel per photon history can be described as [19]:

$$D_{enh} = \frac{1}{m_{vox}} \sum_{i=1}^{N_e} S(E_i) \ell_i \quad (8)$$

in which  $N_e$  is the number of electrons produced by the ionizations inside the voxel,  $S(E_i) \equiv -dE/dx$  is the stopping power,  $\ell_i$  the fraction of the electron's track length that lies inside the voxel, dependent on stochastic mechanisms such as straggling and quasi-elastic interactions, are all positive values. Assuming that both are nearly independent, and considering the geometric central-limit theorem, the product of these variables is log-normally distributed.

The total number of electrons per Gy of baseline dose is  $N_e = N_{ion}^{Gy} \cdot N_{Auger}$ , where  $N_{Auger}$  is the number of Auger electrons produced by an ionization event in the AuNP.

### 3.3. Stochastic form and relation to macroscopic dose

If local dose in the vicinity of the AuNP is log-normally distributed, it follows that

$$D_{enh} = D_0 \exp(\sigma Z), \quad Z \sim \mathcal{N}(0, 1), \quad (9)$$

meaning that for the distribution,

$$\ln \left( \frac{D_{enh}}{D_0} \right) = \sigma Z, \quad (10)$$

$\sigma$  is its standard deviation.

Now, considering that each ionisation that launches an Auger cascade deposits *on average*  $\varepsilon_{cas} N_e$  Gy then

$$D_{extra} = \varepsilon_{cas} N_e, \quad (11)$$

In reality,  $\varepsilon_{cas} N_{Auger}$  likely follows a Poisson distribution; here we simplify by simply using the expectation value.

$D_{extra}$  is the mean additional (macroscopic) dose delivered to the nucleus by all AuNP cascades per 1 Gy of baseline. Using equation 7, this can be rewritten as:

$$D_{\text{extra}} = \varepsilon_{\text{cas}} N_{\text{Auger}} \mathcal{F}(E, t) N_{\text{AuNP}} V_{\text{AuNP}}, \quad (12)$$

such that

$$\langle D_{\text{enh}} \rangle = D_0 + D_{\text{extra}}. \quad (13)$$

Then, the dose enhancement ratio can be written as:

$$\text{DER} = \frac{\langle D_{\text{enh}} \rangle}{D_0} = 1 + \frac{D_{\text{extra}}}{D_0} = 1 + K N_{\text{AuNP}} R^3, \quad (14)$$

Where all the constant terms are flushed into:

$$K(E) = \frac{4\pi}{3} \varepsilon_{\text{cas}} N_{\text{Auger}} \mathcal{F}(E, t), \quad (15)$$

where  $\mathcal{F}(E, t)$  has already been defined in equation 7,  $K(E)$  is a function of energy and comes in units of  $\text{NP}^{-1} \text{nm}^{-3}$ .

If one wants to specify the intracellular concentration  $c$  [mM], knowing that the NP count in one cell is

$$N_{\text{NP}} = c V_{\text{nuc}} \frac{M_{\text{Au}}}{\rho_{\text{Au}}} \frac{3}{4\pi} \frac{1}{R^3}. \quad (16)$$

Replacing equation 16 into equation (14) eliminates the  $R^3$  term and defines a concentration prefactor  $K_c$ :

$$K_c(E) = \varepsilon_{\text{cas}} N_{\text{Auger}} \mathcal{F}(E, t) V_{\text{nuc}} \frac{M_{\text{Au}}}{\rho_{\text{Au}}} \quad [\text{mM}^{-1}]. \quad (17)$$

Hence

$$\text{DER} = 1 + K_c(E) c. \quad (18)$$

This is an interesting finding as it corroborates previous findings that reported dose enhancement was mostly due to concentration. Some authors

reported that smaller AuNPs in higher concentrations closer to the nuclear had more enhancement than larger ones [8]

Finally, knowing that, for a standard normal variable  $Z$ ,  $\mathbb{E}[e^{\sigma Z}] = e^{\sigma^2/2}$  [20], then

$$\langle D_{\text{enh}} \rangle = D_0 e^{\sigma^2/2}. \quad (19)$$

.

Solving for  $\sigma$ , and using equation 14:

$$\sigma^2 = 2 \ln \left( \frac{\langle D_{\text{enh}} \rangle}{D_0} \right) = 2 \ln(\text{DER}) = 2 \ln(1 + K_c c) \quad (20)$$

$$\sigma = \sqrt{2 \ln(1 + K_c c)} \quad (21)$$

Equation 21 shows that the stochastic width  $\sigma$  is now a deterministic function of three measurable quantities: beam-specific  $K_c$  and intracellular molar concentration  $c$ . The particle radius  $R$  dependence disappears, which is consistent with results showing that higher concentrations of smaller AuNPs yield higher DERs than larger AuNPs [8]. No voxel histograms or Monte-Carlo dose maps are required once  $K_c$  has been fixed for the spectrum.

To note that a more rigorous treatment would parameterize the enhanced dose as  $D_{\text{enh}} = D_0 \exp(\mu + \sigma Z)$  with a separate  $(\mu)$  term.

For this more general form, the expectation value would be  $\mathbb{E}[D_{\text{enh}}] = D_0 \exp(\mu + \sigma^2/2)$ , leading to variance scaling of the form  $\sigma^2 = k \ln(1 + K_c c)$ , where  $k$  is a scaling term between 0 and 2. At  $k = 0$ , we would be in a completely deterministic dose shift with  $\sigma = 0$  and the dose enhancement would be strictly due to the mean  $\mu = \ln(1 + K_c c)$ . For  $k = 1$ , the enhancement is split evenly between the deterministic shift and stochastic enhancement. Finally for  $k = 2$ ,  $\mu = 0$ , meaning that we are in the fully stochastic regime and we retrieve equation 21. Values of  $k > 2$  would lead to physically implausible scenarios where the deterministic shift would be negative, and can therefore be discarded.



To maintain consistency with our physically motivated scenario in which dose enhancement arises strictly from increased stochastic fluctuations, the choice  $k = 2$  yields  $\mu = 0$  and  $\sigma^2 = 2 \ln(1 + K_c c)$ , which retrieves our original formulation.

The previously obtained values of  $K_c(E)$ , DER and  $\sigma$  can be directly compared with the values obtained for monoenergetic photon beam irradiated Bovine aortic endothelial cells (BAEC) at different energies (30, 40, 50, 60, 70, 81, and 100 keV) at a concentration of AuNPs of  $c = 1$  mM [21]. The values used to estimate  $K_c$  were  $\rho_{Au} = 19.3 \text{ g cm}^{-3}$ ,  $M_{Au} = 196.97 \text{ g mol}^{-1}$ ,  $V_m = \frac{M_{Au}}{\rho_{Au}} \approx 10.2 \text{ cm}^3 \text{ mol}^{-1}$ , and  $V_{nuc} = 5.0 \times 10^{-11} \text{ cm}^3$ , whereas the photon cross-sections for gold and tissue were taken from the National Institute of Standards and Technology, USA (NIST)[22].

Energy (keV)	DER <sub>exp</sub>	DER <sub>model</sub>	% Diff
30	1.74	4.28	+146.0%
40	3.47	3.52	+1.4%
50	2.77	2.82	+1.8%
60	3.06	2.23	-27.1%
70	1.30	1.78	+36.9%
81	2.58	3.45	+33.7%
100	1.35	2.16	+60.0%

Table 1: DER values obtained using this work’s model and the synchrotron results of [21]

The comparison is presented in table 1, together with a graphical comparison shown in figure 1.

Despite its minimal structure, the present cascade-based model reproduces the published DERs to better than a factor  $\approx 2$  (RMSE  $\approx 0.9$ ), with a clear prediction of the dip at 70 keV. However, there’s some discrepancy in the lower energy DER comparison, perhaps because low-energy measurements ( $\leq 40$  keV) are more sensitive to microdosimetric uncertainties.

The sole free quantity is the product  $\varepsilon_{cas} N_{Auger}$ , i.e. the mean lethal dose delivered to nuclear DNA per gold photo-ionisation. Direct experimental or in-silico estimates for this quantity do not exist; literature values for both  $\varepsilon_{cas}$  ( $10^{-7}$ – $10^{-4} \text{ Gy cascade}^{-1}$ ) and  $N_{Auger}$  (10–30 electrons) span orders of magnitude. Calibrating the product to the synchrotron dataset yields

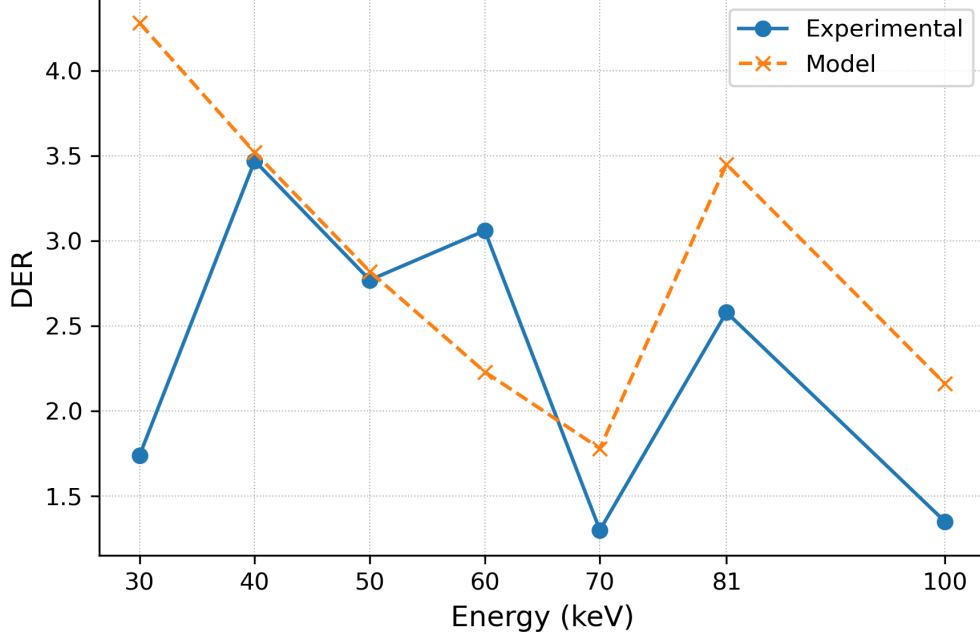


Figure 1: Graphical comparison of model DER vs synchrotron experimental DER

$\epsilon_{cas} N_{Auger} \approx 1 \times 10^{-5} \text{ Gy}$ , well within the plausible range.

In figure 2,  $K_c$  is provided as a function of energy (1keV-20MeV), assuming monoenergetic beam values:

Taken together, the agreement supports the view that a single, energy-independent calibration of  $\epsilon_{cas} N_{Auger}$ , combined with known cross-sections and a realistic nuclear volume, is sufficient to predict DER within experimental scatter.

However, clinical beams are typically not monochromatic and therefore the bracketed terms should be spectrum-weighted.

We determined the value of  $K_c$  for two kilovoltage (kV) spectra - 50 and 100 kVp, determined with SpekPy [23], using an anode angle of  $20^\circ$  and a filtration setup of 0.8 mm of beryllium (Be) + 3.9 mm of aluminum (Al): and for four mega-voltage (MV) spectra as reported by [24].

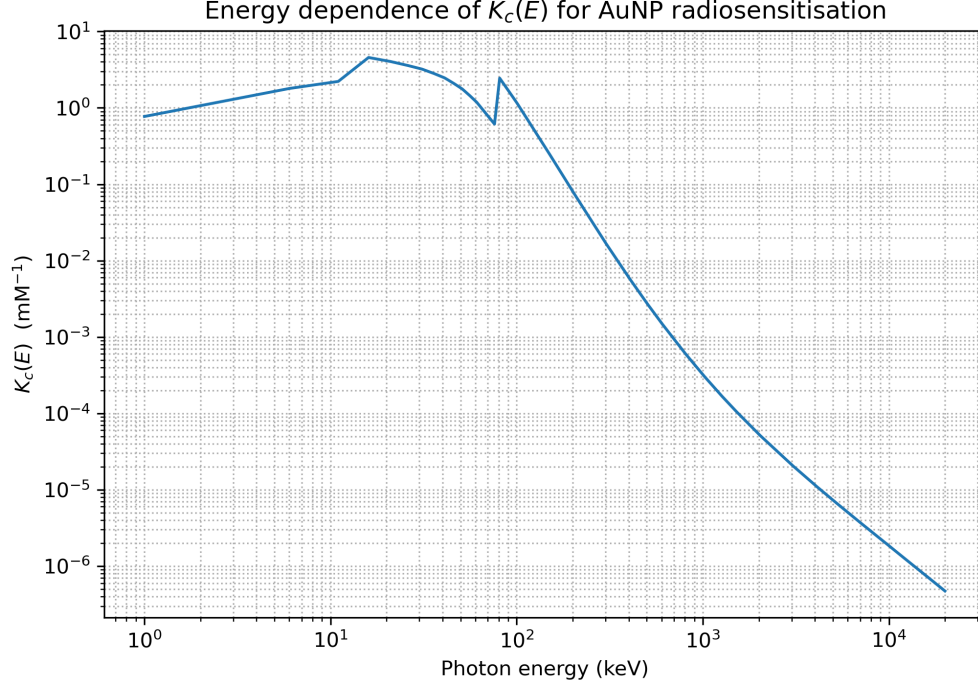


Figure 2:  $K_c(E)$  as a function of energy (keV) in log-log scale

The results are summarized in table 2.

McMahon *et al.* [8] noted that radiosensitisation rises with both total Au mass (concentration) and AuNP volume, in such a way that the  $R^3$  dependence is mitigated if smaller particles in higher quantities are used, which is observed in our model, given that because the  $R^3$  terms cancel out in equation ??, it only depends on the concentration. In table 3 values of DER are given for the spectra for three different concentrations.

It can be seen that for kV beams the DER will be measurable. However, for mega-voltage beams, even with the lower-energy tail, the projected DERs would be negligible according to this model. This seems to contradict several experiments which have shown that DERs are not negligible in MV beams. This sets perhaps a limit of validity to the current model.

Table 2: Spectrum-averaged radiosensitisation constant  $K_c$  for the clinical photon beams used in this work.

Beam	$K_c$ (mM <sup>-1</sup> )
<i>kV beams</i>	
50 kVp	3.22
100 kVp	2.11
<i>MV beams</i>	
Varian 10 MV	$1.23 \times 10^{-4}$
Varian 6 MV	$3.48 \times 10^{-4}$
Siemens 6 MV	$3.72 \times 10^{-4}$
Elekta 6 MV	$3.01 \times 10^{-4}$
Varian 4 MV	$2.24 \times 10^{-4}$

Table 3: DER predicted by  $DER = 1 + K_c c$  for three concentrations in mM

	0.1	0.5	1.0
50 kVp	1.322	2.611	4.222
100 kVp	1.211	2.055	3.111
Varian 10 MV	1.0000123	1.0000615	1.000123
Varian 6 MV	1.0000348	1.000174	1.000348
Siemens 6 MV	1.0000372	1.000186	1.000372
Elekta 6 MV	1.0000301	1.000150	1.000301
Varian 4 MV	1.0000224	1.000112	1.000224

### 3.4. Analytical survival curves

Expanding equation 9 to first order gives [13]:

$$D_{\text{enh}} = D_0(1 + \sigma Z) + \mathcal{O}(\sigma^2), \quad (22)$$

in which we're going to neglect second order terms, the end result is in fact a gaussian distribution

Now we're going to use the linear quadratic model to determine the survival curve for each  $D_{enh}$ :

$$S_{enh} = e^{-\alpha D_{enh} - \beta D_{enh}^2}. \quad (23)$$

Replacing  $D_{enh}$  with equation 22 yields for each term in equation 23 [13]:

$$\begin{aligned} -\alpha D_{enh} &= -\alpha D_0(1 + \sigma Z) = -\alpha D_0 - \alpha \sigma D_0 Z, \\ -\beta D_{enh}^2 &= -\beta D_0^2(1 + 2\sigma Z + \sigma^2 Z^2) \\ &= -\beta D_0^2 - 2\beta \sigma D_0^2 Z - \beta \sigma^2 D_0^2 Z^2. \end{aligned} \quad (24)$$

The cross-term  $2\sigma Z$ , corresponds to a simultaneous energy deposit of both baseline photons and enhanced Auger electrons at the same voxel [5], considered of low probability, therefore, it is often neglected [25].

Neglecting this terms leads to:

$$S_{enh} \approx e^{-\alpha D_0(1+\sigma Z) - \beta D_0^2 - \beta \sigma^2 D_0^2 Z^2}, \quad (25)$$

The macroscopic survival fraction can be obtained by averaging over the Gaussian fluctuations.

$$\begin{aligned} S_\sigma = \langle S_{enh} \rangle &= e^{-\alpha D_0 - \beta D_0^2} \mathbb{E}_Z[e^{-\alpha \sigma D_0 Z - \beta \sigma^2 D_0^2 Z^2}] \\ &= e^{-\alpha D_0 - \beta D_0^2} \frac{\exp\left(\frac{\alpha^2 \sigma^2 D_0^2}{2(1 + 2\beta \sigma^2 D_0^2)}\right)}{\sqrt{1 + 2\beta \sigma^2 D_0^2}}, \end{aligned} \quad (26)$$

where the Gaussian identity  $\mathbb{E}[e^{tZ+bZ^2}] = e^{\frac{t^2}{2(1-2b)}}$  for  $b < \frac{1}{2}$  [20](eq. 7.4.32) was used (derivation given in Supplementary Material).

Also, given that  $b = -\beta \sigma^2 D^2$  is always negative, since  $\beta, \sigma^2, D^2 > 0$ , then  $1 - 2b \geq 1$ , making the hard limit of validity only happen if  $2\beta \sigma^2 D^2 \rightarrow 1$ , or  $\beta \approx \frac{1}{2\sigma^2 D^2}$ , meaning an extremely low value of  $\beta$ .

Finally, in the equation,  $\sigma = \sqrt{2\ln(1 + K_c c)}$ ,  $D_0$  is the baseline dose with no AuNPs, and  $\alpha, \beta$  are the linear and quadratic coefficients of the LQ model.

This equation is completely defined for any given value of  $K_c$  (beam dependent), and the molar concentration  $c$ .

The next step was to test the validity of the model. For that, we used the data provided by [5] as source, with experimental data taken from [7]. These two works were performed on BAECs using different X-ray beam qualities (Brown's work was used to model Rahman's results). Experimental values were extracted by making use of webplotdigitizer [12] which allowed us to retrieve the experimental data points to within two significant figures.

We compared our model against their results, obtained for the 100 kVp beam, for concentrations of 0.00, 0.25, 0.50, and 1.00 mM of AuNPs. The survival curve for our model was determined using equation 26; the pre-calculated  $K_c = 2.11 \text{ mM}^{-1}$  value for our own 100 kVp spectrum, applied for the same concentration values. the LQ baseline values were taken from [5] to be  $\alpha = 2.52 \times 10^{-2} \text{ Gy}^{-1}$  and  $\beta = 1.30 \times 10^{-2} \text{ Gy}^{-2}$  for 1 mM.

The application of equation 26 yielded Dose Enhancement Factors at 80% survival ( $\text{DEF}_{80\%}$  of 1.12, 1.18 and 1.27, with a percent deviation of -4%, -20%, and -32% to the reported values [5, 7] of 1.17, 1.47 and 1.94. This means the model was well calibrated to the lower concentration value (0.25 mM), but failed for the other two concentrations (0.50 and 1.00 mM).

So, we decided to reintroduce the term  $2\sigma Z$ , meaning that we're now considering that higher concentrations increase the probability of double baseline+enhance dose deposition in the same site. If one collects the terms of same order of  $Z$  from equation 24, we can see that equations 25 and 26 can be rewritten as:

$$\begin{aligned} S_{enh} &= e^{-\alpha D_0 - \alpha \sigma D_0 Z - 2\beta \sigma D_0^2 Z - \beta D_0^2 - \beta \sigma^2 D_0^2 Z^2} \\ &= e^{-\alpha D_0 - \beta D_0^2} e^{-(\alpha - 2\beta D_0) \sigma D_0 Z - \beta D_0^2}, \end{aligned} \quad (27)$$

where  $\alpha^* = \alpha + 2\beta D_0$ . The equation is formally similar to 26 before averaging to obtain the macroscopic curve, leading to:

$$\begin{aligned}
S_{\sigma}^{\text{mixed}} &= \langle S_{enh} \rangle = e^{-\alpha D_0 - \beta D_0^2} \mathbb{E}_Z[e^{-\alpha^* \sigma D_0 Z - \beta \sigma^2 D_0^2 Z^2}] \\
&= e^{-\alpha D_0 - \beta D_0^2} \frac{\exp\left(\frac{\alpha^{*2} \sigma^2 D_0^2}{2(1 + 2\beta \sigma^2 D_0^2)}\right)}{\sqrt{1 + 2\beta \sigma^2 D_0^2}}. \tag{28}
\end{aligned}$$

Applying this model to the curves yielded DEFs<sub>80%</sub> of 1.30 (10.1%) for the 0.25 M concentration, 1.51 (5.6%) for the 0.50 mM concentration, and 1.70 (-6.1%) for the 1.00 mM concentration. Percent deviates are in parenthesis.

It's clear that the insertion of the mixed term contributed to an improvement of the DEFs<sub>80%</sub> for higher concentrations, while making it worse for the lowest concentration, meaning that at lower loads, the mixed term is indeed negligible, but this is no longer the case for the higher 0.50 and 1.00 mM loads.

Yet, at higher concentrations the values were still lagging lower than necessary. A hypothesis can be formulated that not only the probability of a double baseline/enhanced dose deposition increases, but the probability of two simultaneous cascade derived dose depositions on the same site also increases, which was not accounted for in this variance-only derivation.

To account for the two simultaneous hits, the Taylor expansion 9 was increased to up to second order:

$$D_{\text{enh}} = D_0(1 + \sigma Z + \frac{1}{2}\sigma^2 Z^2) + \mathcal{O}(\sigma^3). \tag{29}$$

Reintroducing this into equation 23:

$$\begin{aligned}
-\alpha D_{\text{enh}} &= -\alpha D_0 \left(1 + \sigma Z + \frac{1}{2} \sigma^2 Z^2\right) = -\alpha D_0 - \alpha \sigma D_0 Z - \frac{1}{2} \alpha \sigma D_0^2 Z^2, \\
-\beta D_{\text{enh}}^2 &= -\beta D_0^2 \left(1 + \sigma Z + \frac{1}{2} \sigma^2 Z^2\right)^2 \\
&= -\beta D_0^2 \left(1 + 2 \sigma Z + 2 \sigma^2 Z^2 + \sigma^3 Z^3 + \frac{1}{2} \sigma^4 Z^4\right) \\
&\approx -\beta D_0^2 - 2 \beta \sigma D_0^2 Z - 2 \beta \sigma^2 D_0^2 Z^2.
\end{aligned} \tag{30}$$

In which we specifically dropped the terms of higher order than  $\mathcal{O}(\sigma^2)$ .

Now we can collect the terms of equal powers of  $Z$ :

$$\begin{aligned}
-\alpha D_{\text{enh}} - \beta D_{\text{enh}}^2 &= (-\alpha D_0 - \beta D_0^2) + \\
&\quad + \sigma (-\alpha D_0 - 2 \beta D_0^2) Z + \sigma^2 \left(-\frac{1}{2} \alpha D_0^2 - 2 \beta D_0^2\right) Z^2. \tag{31}
\end{aligned}$$

Defining:

$$\begin{aligned}
a &= -\sigma D_0 (\alpha + 2 \beta D_0) = -\sigma D_0 \alpha^* \\
b &= -\sigma^2 D_0 \left(\frac{1}{2} \alpha + 2 \beta D_0\right).
\end{aligned} \tag{32}$$

and averaging to obtain the macroscopic survival, yields:

$$S_{\sigma^2} = e^{-\alpha D_0 - \beta D_0^2} \mathbb{E}[e^{aZ + bZ^2}], \tag{33}$$

thus being reduced to the integrable Gaussian form. Performing the integration and replacing the values leads to:

$$S_{\sigma^2} = \frac{\exp\left(-\alpha D_0 - \beta D_0^2 + \frac{\sigma^2 D_0^2 (\alpha + 2 \beta D_0)^2}{2[1 + \sigma^2 D_0 (\alpha + 4 \beta D_0)]}\right)}{\sqrt{1 + \sigma^2 D_0 (\alpha + 4 \beta D_0)}} \tag{34}$$

Using this survival curve to determine DEFs<sub>80%</sub> on the three different concentrations, yielding the values of 1.42 (+21.6%), 1.68 (+14.2%) and 2.01



(+3.6%), respectively, with the percent deviations to experimental values in parenthesis.

With this analysis, it becomes clear that the optimal models for each concentration are:

- for 0.25 mM, the first-order approximation excluding the mixed term;
- for 0.50 mM, the first-order approximation including the mixed term;
- for 1.00 mM, the second order approximation

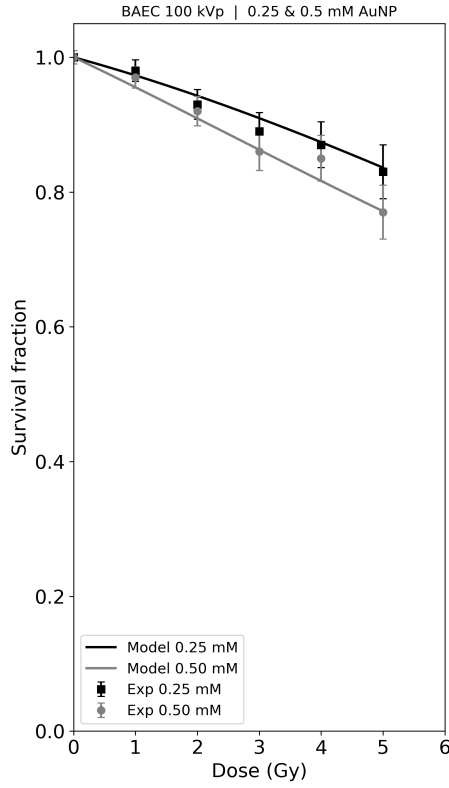
### 3.5. Model Survival curve comparison for 100 kVp BAEC

In figure 4 we present the baseline LQ control fitted with  $S_\sigma$  for ( $\sigma = 0$ ) and the  $S_{\sigma^2}$  model for the 1.00 mM concentration, and in figure 3 we compare the and the  $S_\sigma^{mixed}$  model curves to the 0.25 mM and 0.50 mM datasets, respectively, side by side with Brown's results for the 100 kVp beam.

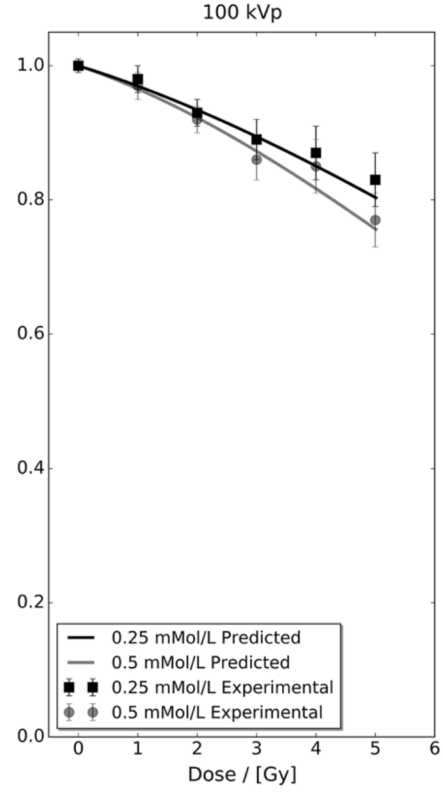
A graphical analysis shows that the obtained survival curves explain the experimental points within a small uncertainty, confirmed by the experimental survival fraction values obtained from [5, 7] compared with the results using our models, shown in table 4.

It is noticeable that all results fall below percent deviations smaller than 2% except for one value at 3.9% for the 0.50 mM concentration at 4.0 Gy.

Despite the good results of the model, figures ?? show the obtained survival curves for this show some significant graphical changes to the LEM curves, which show more curvature.

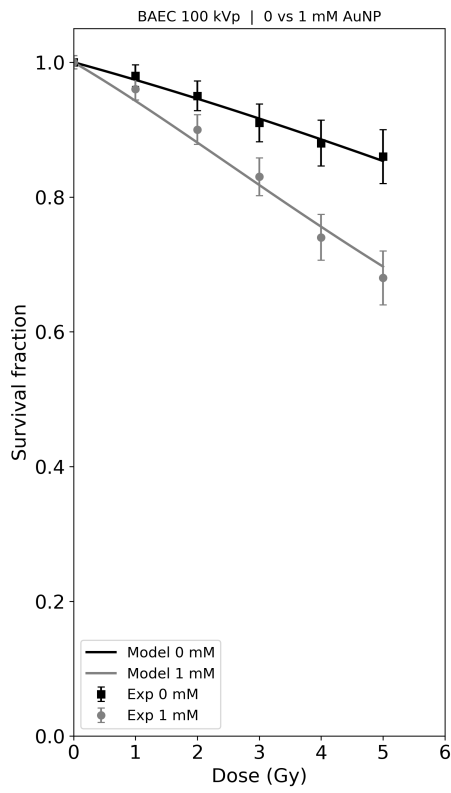


(a) Results for 0.25 mM and 0.50 using the  $S_{\sigma}$  and  $S_{\sigma}^{mixed}$  survival curve models, respectively.

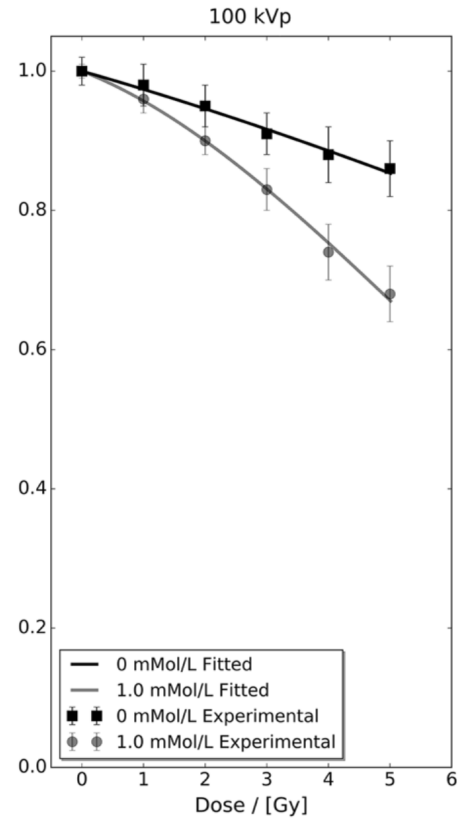


(b) Results using the LEM for the same concentrations, taken from [5].

Figure 3: Graphical comparison between the analytical models and the LEM [5] for 0.25 and 0.50 mM concentrations



(a) Results for 0.00 mM and 1.00 using the  $S_\sigma$  (for  $\sigma = 0$  and  $S_{\sigma^2}$  survival curve models, respectively).



(b) Results using the LEM for the same concentrations, taken from [5].

Figure 4: Graphical comparison between the analytical models and the LEM [5] for 0.00 and 1.00 mM concentrations

Dose (Gy)	0 mM			0.25 mM			0.50 mM			1.00 mM		
	SF <sub>exp</sub>	SF <sub>model</sub>	% dev	SF <sub>exp</sub>	SF <sub>model</sub>	% dev	SF <sub>exp</sub>	SF <sub>model</sub>	% dev	SF <sub>exp</sub>	SF <sub>model</sub>	% dev
0.0	1.00	1.0000	0.0	1.00	1.0000	0.0	1.00	1.0000	0.0	1.00	1.0000	0.0
1.0	0.98	0.9738	-0.6	0.98	0.9730	-0.7	0.97	0.9554	-1.5	0.96	0.9427	-1.8
2.0	0.95	0.9459	-0.4	0.93	0.9428	1.4	0.92	0.9093	-1.2	0.90	0.8808	-2.1
3.0	0.91	0.9164	0.7	0.89	0.9096	2.2	0.86	0.8626	0.3	0.83	0.8178	-1.5
4.0	0.88	0.8855	0.6	0.87	0.8739	0.5	0.85	0.8165	-3.9	0.74	0.7559	2.2
5.0	0.86	0.8534	-0.8	0.83	0.8362	0.7	0.77	0.7715	0.2	0.68	0.6968	2.5

Table 4: Experimental and model survival fractions (SF) and percentage differences for each AuNP concentration.

Table 5 lists the  $\alpha', \beta'$  pairs obtained by fitting the analytic survival curves with a linear-quadratic law  $\ln S = -\alpha'D - \beta'D^2$  using a  $D^2$ -weighted least-squares fit in linear space. Errors are  $1\sigma$  from the covariance matrix;  $R^2 > 0.998$  in all cases.

Conc. (mM)	$\alpha'$ ( $\text{Gy}^{-1}$ ) $\pm\text{SE}$	$\beta'$ ( $\text{Gy}^{-2}$ ) $\pm\text{SE}$	$R^2$	Brown (100 kVp)	
				$\alpha'$	$\beta'$
0.00	$0.0252 \pm 0.0000$	$0.00130 \pm 0.0000$	1.000	–	–
0.25	$0.0253 \pm 0.0000$	$0.00209 \pm 0.0000$	1.000	–	–
0.50	$0.0459 \pm 0.0001$	$0.00118 \pm 0.0000$	0.999	–	–
1.00	$0.0606 \pm 0.0004$	$0.00230 \pm 0.0001$	0.999	0.0347	0.00904

Table 5: LQ parameters fitted to the  $\sigma$ -LEM curves. The last column shows Brown’s empirical 1.00 mM pair for comparison.

At 1 mM the analytic curve yields  $(\alpha', \beta') = (0.0606, 0.00240)$ , completely different from the values of  $(0.0347, 0.00904)$ , from [5]. This difference will be exploited further in the discussion section.

#### 4. Discussion

During derivation, we treated  $\varepsilon_{\text{cas}}N_{\text{Auger}}$  as an energy-independent constant. This is a first-order simplification: the number of primary photo-ionisations in a nanoparticle is likely Poisson-distributed and therefore energy-dependent, so future work should focus on a systematic, energy-resolved derivation, ideally guided by Monte-Carlo results.

A mid-step in the derivation of the survival curves was the calculation of the beam quality constant  $K_c$ , which due to the value  $\varepsilon_{\text{cas}}N_{\text{Auger}}$  being unknown to good accuracy, was calibrated against synchrotron monoenergetic beam results. Results showed that  $K_c$  peaks in the kV range ( $3.22 \text{ mM}^{-1}$  at 50 kVp,  $2.11 \text{ mM}^{-1}$  at 100 kVp) and fall to  $\mathcal{O}(10^{-4}) \text{ mM}^{-1}$  for MV spectra, yet faithfully reproducing the measured dip at 70 keV, related with gold’s L3 / K-edges. The unrealistic DER predictions at the MV regime point to the current formalism’s limitation to  $\lesssim 150 - 200 \text{ keV}$ .

The derivation of the survival curves relied on assuming a log-normal distribution for the dose enhancement, driven solely by stochasticity. Although a closed-form is not attainable using the log-normal distribution, Taylor expansion to first and second order, with inclusion or exclusion of terms, allowed for the development of three variants of the model, the  $S_\sigma$  is adapted for low concentration regimes, with sparse local dose enhancements, dominated by single Auger cascade hits and low probability of a simultaneous baseline and Auger cascade hit happening on the same site as being negligible. The  $S_\sigma^{mixed}$  model is adapted to an intermediate concentration level, where although still dominated by single Auger cascade hits, the mixed term related to the simultaneous hit above can no longer be neglected. Finally, the  $S_{\sigma^2}$  model is adapted to higher concentrations. Here the Taylor expansion is taken to second order, therefore we assume that single and double Auger cascade hits can dominate the dose enhancement.

The models were compared with previous results obtained for BAEC cells irradiated with 100 kVp, both with experimental and LEM derived data. Although the x-ray spectrum used for the BAEC results was different from the spectrum we used for our model, the value of  $K_c = 2.11 \text{ mM}^{-1}$  was well adapted to the results.

The models used were able to reproduce  $\text{DEF}_{80\%}$  within  $\pm 5\%$ . The variance, mixed and second-order curves optimise the 0.25, 0.50 and 1.00 mM datasets, respectively. Fitted LQ parameters reveal a marked rise in  $\alpha'$  with almost unchanged  $\beta'$ , showing that enhancement is predominantly  $\alpha$ -driven and less curved than standard LEM predictions. In fact, in our model, we assume that  $\varepsilon_{\text{cas}} N_{\text{Auger}}$  leads to single Auger cascades producing single-track events, with or without a mixed term which also deals with single-track hits probability of being simultaneous with a baseline hit, in fact the mixed term introduction lowers  $\beta'$  as it literally implies a growth in  $\alpha$  by  $2\beta D_0$ . Two cascades must overlap to improve upon  $\beta$ , which is impossible in the  $S_\sigma$  and the  $S_\sigma^{mixed}$  models. Only in the second-order expansion are double cascades accounted for, which explains the jump in  $\beta'$  in the results, thus the models on these concentration ranges and beam quality seem to indicate radiosensitisation is chiefly  $\alpha$ -driven, with  $\beta$  playing only a secondary role at the only concentration deemed high (1.00 mM). This is a stark contrast with the LEM, which is in fact blind to this issue as it scores the dose depositions regardless of their origin and then average over the entire domain. The  $\sigma$ -LEM model

exposes exactly where  $\beta$  dominated events become relevant (at second-order,  $\sigma^2$  terms), pointing to a more physical interpretation that indeed at lower concentrations, the sparser Auger cascade-driven enhancement has a lower probability of two  $\beta$ -style double-hits, which only become relevant at higher concentrations.

## 5. Conclusions

The analytical  $\sigma$ -LEM was succesful in modelling the BAEC experimental results, with  $DEF_{80\%}$  below 5% for all concentration regimes, and reproducing survival curves with percent deviations to the experimental values smaller than 2%, except for one point.

Closed-form expressions for the survival curves were attainable by expanding to first- and second-order moments of the log-normal distribution. The three variants of the model, for low, intermediate and high concentrations, reveal that sensitisation is mainly  $\alpha$ -driven, at-least until the high concentration regime

The great advantage of this model is that it collapses radiosensitisation to a beam-quality related factor,  $K_c(E)$ , and intracellular concentration  $c$ . It also makes predictions based solely on physical principles perhaps allowing for better insights relative to the physical mechanisms behind dose enhancement.

Uncertainty in the  $K_c(E)$  value entailed the need to calibrate it to synchrotron monoenergetic data.

Finallt the fact that the model predicts DERs close to 1 in the MV range indicates a limit of validity of the model. .

Future work will refine the treatment of  $\varepsilon_{\text{cas}}N_{\text{Auger}}$ , attempt to model the MV regimes, and most importantly, test the formalism for other beam qualities, cell lines, and in-vitro/in-silico scenarios.

## References

- [1] W. Li, et al., Intercomparison of monte carlo simulation approaches for dose enhancement by gold nanoparticles, *Physica Medica* 76 (2020) 116–123. doi:10.1016/j.ejmp.2020.07.015.
- [2] W. B. Li, M. Beuve, S. D. Maria, W. Friedland, B. Heide, A. P. Klapproth, C. Y. Li, F. Poignant, H. Rabus, B. Rudek, J. Schuemann, C. Villagrasa, Corrigendum to “intercomparison of dose enhancement ratio and secondary electron spectra for gold nanoparticles irradiated by x-rays calculated using multiple monte carlo simulation codes” [*phys. med.* 69 (2020) 147–163], *Physica Medica* 80 (2020) 383–388. doi:10.1016/j.ejmp.2020.11.011.
- [3] H. Rabus, P. Hepperle, C. Schlueter, A. Hloskovsky, W. Y. Baek, Experimental benchmark data for monte carlo simulated radiation effects of gold nanoparticles. part i: Experiment and raw data analysis, *Physica Scripta* 98 (5) (2023) 055015. doi:10.1088/1402-4896/accb14.
- [4] L. Thomas, M. Schwarze, H. Rabus, Radial dependence of ionization clustering around a gold nanoparticle irradiated by x-rays under charged particle equilibrium, *Physics in Medicine and Biology* 69 (18) (2024). doi:10.1088/1361-6560/ad6e4f.
- [5] J. M. C. Brown, F. J. Currell, A local effect model-based interpolation framework for experimental nanoparticle radiosensitisation data, *Cancer Nanotechnology* 8 (1) (2017) 1. doi:10.1186/s12951-016-0025-6.
- [6] B. Chithrani, S. Jelveh, F. Jalali, M. van Prooijen, C. Allen, R. Bristow, R. Hill, D. Jaffray, Radiation enhancement with gold nanoparticles, *Radiation Research* (2010).
- [7] W. Rahman, et al., Gold nanoparticles for x-ray therapy, *Nanomedicine* (2009).
- [8] S. J. McMahon, W. B. Hyland, M. F. Muir, S. Jain, K. T. Butterworth, G. Schettino, G. R. Dickson, A. R. Hounsell, J. M. O’Sullivan, K. M. Prise, Radiobiological consequences of nanoscale energy deposition near irradiated gold nanoparticles, *Scientific Reports* 1 (2011) 18. doi:10.1038/srep00018.



- [9] E. Lechtman, N. Chattopadhyay, Z. Cai, S. Mashouf, R. M. Reilly, J.-P. Pignol, Development and characterization of a monte carlo local effect model (lem) to predict cellular survival after gold nanoparticle-enhanced radiotherapy, *Physics in Medicine and Biology* 58 (10) (2013) 3075–3087. doi:10.1088/0031-9155/58/10/3075.
- [10] C. Kirkby, E. Ghasroddashti, R. Mackay, Dosimetric consequences of gold nanoparticle clustering during radiation therapy, *Medical Physics* 44 (1) (2017) 595–604. doi:10.1002/mp.12030.
- [11] J. Wu, L. Smith, B. Kavanagh, et al., Biological modeling of gadolinium-based nanoparticle radio-enhancement for kilovoltage photons: A monte carlo study, *Cancer Nanotechnology* 14 (2023) 47. doi:10.1186/s12645-023-00201-1.
- [12] A. Rohatgi, Webplotdigitizer, <https://apps.automeris.io/wpd4/>, version 4.8 (accessed 2025-06-05) (2024).
- [13] P. Teles, C. Dias, J. H. Belo, C. Sousa, P. Boaventura, I. Bravo, J. Santos, M. Rylander, Monte carlo simulation and dosimetric analysis of gold nanoparticles (aunps) in breast tissue, arXiv preprint arXiv:2506.01878Submitted to *Radiation Physics and Chemistry* (2025). arXiv:2506.01878.  
URL <https://doi.org/10.48550/arXiv.2506.01878>
- [14] Z. R. Prieskorn, J. E. Hill, P. E. Kaaret, J. K. Black, K. Jahoda, Gas gain measurements from a negative ion tpc x-ray polarimeter, *IEEE Transactions on Nuclear Science* 58 (4) (2011) 2055–2059. doi:10.1109/TNS.2011.2155083.
- [15] Z. R. Prieskorn, J. E. Hill, P. E. Kaaret, J. K. Black, Photoelectron track length distributions measured in a negative ion time projection chamber, *IEEE Trans. Nucl. Sci.* 61 (2) (2014) 894–900. arXiv:1406.4393, doi:10.1109/TNS.2014.2312107.
- [16] H. Sakurai, S. Gunji, F. Tokanai, Photoelectron track image of capillary gas proportional counter, *Nuclear Instruments and Methods in Physics Research Section A: Accelerators, Spectrometers, Detectors and Associated Equipment* 505 (1–2) (2003) 219–222. doi:10.1016/S0168-9002(03)01056-8.

- [17] P. Soffitta, E. Costa, G. di Persio, E. Morelli, A. Rubini, M. Frutti, M. Cocco, M. Trifoglio, G. di Cocco, F. Gianotti, Astronomical x-ray polarimetry based on photoelectric effect with microgap detectors, *Nuclear Instruments and Methods in Physics Research Section A: Accelerators, Spectrometers, Detectors and Associated Equipment* 469 (2001) 164–176. [arXiv:astro-ph/0012183](#), [doi:10.1016/S0168-9002\(01\)00772-0](#).
- [18] J. H. Miller, M. T. Batdorf, D. J. Lynch, R. R. Lewis, W. E. Wilson, Microdosimetry of electron microbeams, *Radiation Research* 162 (4) (2004) 474–479. [doi:10.1667/rr3242](#).
- [19] J. F. Williamson, Monte carlo evaluation of kerma at a point for photon transport problems, *Medical Physics* 14 (4) (1987) 567–576. [doi:10.1118/1.596069](#).
- [20] M. Abramowitz, I. A. Stegun (Eds.), *Handbook of Mathematical Functions with Formulas, Graphs, and Mathematical Tables*, Dover Publications, New York, 1965.
- [21] W. N. Rahman, S. Corde, N. Yagi, S. A. A. Aziz, N. Annabell, M. Geso, Optimal energy for cell radiosensitivity enhancement by gold nanoparticles using synchrotron-based monoenergetic photon beams, *International Journal of Nanomedicine* 9 (2014) 2459–2467. [doi:10.2147/IJN.S59471](#).
- [22] J. H. Hubbell, S. M. Seltzer, Tables of x-ray mass attenuation coefficients and mass energy-absorption coefficients 1 keV to 20 MeV for elements  $Z = 1$  to 92 and 48 additional substances of dosimetric interest, <https://physics.nist.gov/PhysRefData/XrayMassCoef/>, version 1.4, National Institute of Standards and Technology, Gaithersburg, MD (2004).
- [23] G. Poludniowski, S. Evans, M.-L. Cremers, D. C. Shipley, R. B. Amos, Spekpy: a python toolkit for modelling x-ray spectra, *Physics in Medicine and Biology* 64 (7) (2019) 075013. [doi:10.1088/1361-6560/ab06d3](#).
- [24] D. Sheikh-Bagheri, D. W. O. Rogers, Monte carlo calculation of nine megavoltage photon beam spectra using the beam code, *Medical Physics* 29 (3) (2002) 391–402. [doi:10.1118/1.1445413](#).

- [25] E. Lechtman, J. Pignol, Interplay between the gold nanoparticle sub-cellular localization, size, and the photon energy for radiosensitization, Sci. Rep. 7 (2017) 13268. doi:10.1038/s41598-017-13736-y.

## Supplementary Material

### Appendix A. Expansion of $\mathbb{E}_Z[e^{-\alpha\sigma D_0 Z - \beta\sigma^2 D_0^2 Z^2}]$

In this section we will that the following identity holds:

$$\mathbb{E}_Z \left[ e^{tZ+bZ^2} \right] = \frac{1}{\sqrt{1-2b}} \exp \left( \frac{t^2}{2(1-2b)} \right), \quad b < \frac{1}{2}$$

The expectation value of a  $f(Z)$  in which  $Z \sim \mathcal{N}(0, 1)$  can be written as:

$$\mathbb{E}_{f(Z)} = \frac{1}{\sqrt{2\pi}} \int_{-\infty}^{\infty} f(z) e^{-\frac{z^2}{2}} dz.$$

Replacing

$$\mathbb{E} \left[ e^{tZ+bZ^2} \right] = \frac{1}{\sqrt{2\pi}} \int_{-\infty}^{\infty} e^{tz+bz^2-\frac{z^2}{2}} dz = \frac{1}{\sqrt{2\pi}} \int_{-\infty}^{\infty} e^{-(az^2+bz)+c} dz,$$

where  $c = \frac{t^2}{2(1-2b)}$  is constant in  $z$ , and can therefore be taken out of the integral, leaving:

$$\mathbb{E} \left[ e^{tZ+bZ^2} \right] = \frac{1}{\sqrt{2\pi}} e^c \int_{-\infty}^{\infty} e^{-(az^2+bz)} dz$$

From equation 7.4.32[20]:

$$\int e^{-(az^2+bz)} dz = \sqrt{\frac{\pi}{a}} \operatorname{erf} \left( \sqrt{a}z + \frac{b}{2\sqrt{a}} \right) + \text{const.}$$

For the definite integral over  $(-\infty, \infty)$ , the error function term simplifies (as when  $z \rightarrow +\infty$ ,  $\operatorname{erf}(f(z)) \rightarrow 1$ , and vice-versa,  $z \rightarrow -\infty$ ,  $\operatorname{erf}(f(z)) \rightarrow -1$ , and we obtain:

$$\int_{-\infty}^{\infty} e^{-(az^2+bz)} dz = \sqrt{\frac{\pi}{a}} \exp \left( \frac{b^2}{4a} \right), \quad a > 0$$

Using  $a = \frac{1}{2} - b$ ,  $b = -t$ , we compute:

$$\mathbb{E} \left[ e^{tZ+bZ^2} \right] = \frac{1}{\sqrt{2\pi}} \int_{-\infty}^{\infty} e^{tz+bz^2-\frac{z^2}{2}} dz = \frac{1}{\sqrt{2\pi}} \sqrt{\frac{\pi}{\frac{1}{2}-b}} \exp \left( \frac{t^2}{4 \left( \frac{1}{2} - b \right)} \right)$$

Simplifying:

$$= \frac{1}{\sqrt{1-2b}} \exp \left( \frac{t^2}{2(1-2b)} \right)$$

Thus confirming:

$$\mathbb{E}_Z \left[ e^{tZ+bZ^2} \right] = \frac{1}{\sqrt{1-2b}} \exp \left( \frac{t^2}{2(1-2b)} \right), \quad b < \frac{1}{2}$$

which follows directly from evaluating the Gaussian integral using the identity in DLMF 7.4.32 and normalizing by the standard normal density.

The integral for the second-order moment can be reduced to a similar form.

## Appendix B. Breakdown of the Dose Enhancement Factor at 80% survival results

Table B.6: DEF<sub>80</sub> comparison across  $\sigma$ -LEM model hierarchy. Baseline D<sub>80</sub> = 6.605 Gy.

Conc. (mM)	Exp. DEF <sub>80</sub>	$\sigma$ -LEM Models		
		Variance	Mixed	Complete 2nd
0.25	1.170	1.116	1.306	1.422
0.50	1.470	1.185	1.514	1.679
1.00	1.940	1.271	1.797	2.011

## Appendix C.

Table B.7: Percentage errors relative to experimental  $\text{DEF}_{80}$  values.

<b>Conc. (mM)</b>	<b>Variance Error (%)</b>	<b>Mixed Error (%)</b>	<b>Complete 2nd Error (%)</b>
0.25	-4.6	+11.6	+21.6
0.50	-19.4	+3.0	+14.2
1.00	-34.5	-7.4	+3.7

Table B.8: Best performing model for each concentration (lowest absolute error).

<b>Concentration (mM)</b>	<b>Best Model</b>	<b>Error (%)</b>
0.25	Variance-only	-4.6
0.50	Mixed term	+3.0
1.00	Complete 2nd order	+3.7